PCCP



PAPER View Article Online
View Journal | View Issue



Cite this: Phys. Chem. Chem. Phys., 2020, 22, 20914

Strain tuned high thermal conductivity in boron phosphide at nanometer length scales — a first-principles study†

Rajmohan Muthaiah 🕩 and Jivtesh Garg 🕩 *

Breakdown of Fourier law of heat conduction at nanometer length scales significantly diminishes thermal conductivity, leading to challenges in thermal management of nanoelectronic applications. In this work we demonstrate using first-principles computations that biaxial strain can enhance k at a nanoscale in boron phosphide (BP), yielding nanoscale k values that exceed even the bulk k value of silicon. At a length scale of k = 200 nm, k = 200 nm, k = 200 of k = 200 nm, k

Received 10th July 2020, Accepted 20th August 2020

DOI: 10.1039/d0cp03690k

rsc.li/pccp

Introduction

As the system length scale diminishes to nanometers, phonon scattering at boundaries becomes pronounced, dramatically decreasing the effective thermal conductivity (k) below the bulk value (Fourier limit).1 This diminished heat transfer at a nanoscale can lead to overheating and a decrease in reliability and performance in nanoelectronic applications. 1,2 A size-dependent decrease in thermal conductivity has been reported experimentally in both bulk and nanomaterials.³⁻⁶ To improve the heat dissipation at a nanoscale, there is a strong need for materials with enhanced thermal conductivity at these length scales. In this work, we show using first-principles computations that biaxial strain can significantly enhance the thermal conductivity of boron phosphide at a nanoscale, yielding nanoscale k values that even exceed the bulk k value of silicon. These results have important implications for achieving efficient thermal management in nanoelectronic applications.

Materials like boron-phosphide (BP) have a large phonon band gap in their vibration spectra due to a large mismatch in masses of the constituent atoms. In recent years, such a phonon gap has been shown to suppress the scattering of acoustic phonons by optical phonons, enhancing the phonon lifetimes, and thus thermal conductivity^{7–13} in a wide range of materials.

School of Aerospace and Mechanical Engineering, University of Oklahoma, Norman, OK 73019, USA. E-mail: garg@ou.edu

In particular, the effect was shown to lead to a thermal conductivity approaching $\sim 1000 \text{ W m}^{-1} \text{ K}^{-1}$ in boron arsenide (BAs). 7,10,12,14 This effect can be understood by observing that anharmonic scattering of phonons through the lowest-order three phonon processes can be classified into two categories an absorption scattering process, where a phonon mode $(q\omega)$ scatters by absorbing another phonon mode $(q'\omega')$, yielding a higher energy ($q''\omega''$) phonon mode, and a decay process, where a phonon mode decays into two lower energy phonons. These processes satisfy energy and momentum conservation given by, $\omega + \omega' = \omega''$ (energy) and $\mathbf{q} + \mathbf{q}' = \mathbf{q}''$ (momentum) for the absorption process and $\omega = \omega' + \omega''$ (energy) and $\mathbf{q} = \mathbf{q}' + \mathbf{q}''$ (momentum) for the decay process. Fig. 1 shows that in silicon, an acoustic phonon $(q\omega)$ can scatter by absorbing another acoustic phonon $(\mathbf{q}'\omega')$ to yield an optical phonon $(\mathbf{q}''\omega'')$, satisfying both momentum and energy conservation. However, in boron-arsenide (BAs), the large phonon gap implies that the third phonon required for energy conservation does not exist, forbidding this scattering process. Such a suppression of scattering of acoustic phonons dramatically enhances the lifetime and thermal conductivity. BP was recently demonstrated to exhibit high bulk k in the range of $\sim 600 \text{ W m}^{-1} \text{ K}^{-1}.^{12,15-17}$

Strain can further enhance k by increasing the phonon band gap, thus further suppressing the scattering of acoustic phonons leading to even higher phonon lifetimes. Lindsay $et\ al.^{17}$ demonstrated the effect of isotropic strain on bulk k enhancement through first-principles computations. Compressive strain was revealed to suppress the above-presented scattering

[†] Electronic supplementary information (ESI) available. See DOI: 10.1039/d0cp03690k

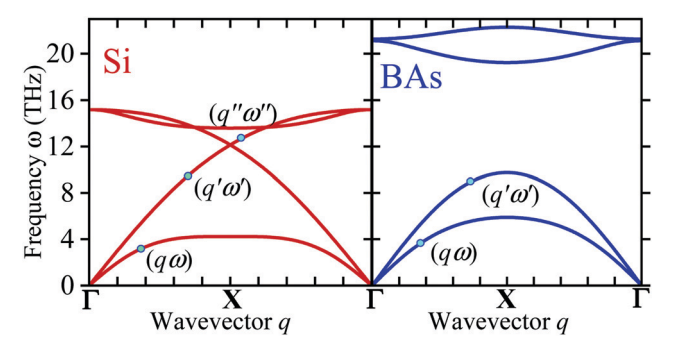


Fig. 1 Phonon dispersions of silicon and boron-arsenide showing the effect of phonon band gap on suppressing anharmonic scattering of acoustic phonons

channel in materials like magnesium oxide (MgO) and silicon carbide (SiC), enhancing their bulk k.

While the above-mentioned work addressed bulk k, in this work we demonstrate that in materials with a phononic band gap, strain can specifically enhance k at a nanoscale. To understand this, it should be noted that k contribution of a phonon mode is proportional to its meanfreepath, Λ ($k \propto \Lambda$). Meanfreepaths typically decrease with an increase in the frequency, being in microns at lower frequencies, and decreasing to nanometer values as frequencies increase. Strain suppresses the anharmonic scattering of phonons at frequencies larger than the magnitude of the phonon band gap (\sim high frequencies). At these frequencies, phonon meanfreepaths are potentially in the nanometer range; suppression of scattering thus enhances Λ in the nanometer range, directly contributing to k enhancement at a nanoscale. The outlined effect, demonstrated in this work, can lead to novel pathways for improving the thermal management at nanometer length scales in a wide range of applications. We demonstrate this effect in BP using first-principles approach as outlined below. We first describe the first-principles approach, followed by thermal conductivity results and analysis.

The first-principles approach 18-21 for predicting thermal conductivity involves exactly solving the phonon Boltzmann transport equation (PBTE). 18 The most important ingredients, namely the 2nd and 3rd order interatomic force constants (IFCs), needed for k prediction, are derived from density-functional theory (DFT).22,23 DFT has been shown to yield highly accurate IFCs, overcoming the limitations of empirical potentials, leading to unprecedented accuracy 20 in the prediction of lattice k. For analysis and discussion, it is useful to present the expression for thermal conductivity (k), predicted based on solving PBTE²¹ in the single mode relaxation time (SMRT) approximation, as given below²⁴ (typically providing a good estimate of k),

$$k_{\alpha} = \frac{\hbar^2}{N\Omega k_{\rm B} T^2} \sum_{\lambda} v_{\alpha\lambda}^2 \omega_{\lambda}^2 \bar{n}_{\lambda} (\bar{n}_{\lambda} + 1) \tau_{\lambda} \tag{1}$$

where α , \hbar , Ω , $k_{\rm B}$, and T, are the Cartesian direction, Planck constant, unit cell volume, Boltzmann constant, and absolute temperature, respectively. λ represents the vibrational mode (qi) (q is the wave vector and j represents phonon polarization). N is the size of the q mesh used for summation in the above equation. ω_{λ} \bar{n}_{λ} , and $v_{\alpha\lambda}$ (= $\partial\omega/\partial q$) are the phonon frequency, equilibrium Bose-Einstein population and group velocity along Cartesian direction α , respectively of a phonon mode λ . These are derived from the knowledge of phonon dispersion computed using 2nd order IFCs. τ_{λ} is the phonon lifetime (equal to the inverse of scattering rate). In the SMRT approximation, the phonon lifetime (τ_{λ}) of a vibrational mode λ is computed using the following equation,

$$\frac{1}{\tau_{\lambda}} = \pi \sum_{\vec{\lambda}, \vec{\lambda}''} |V_3(-\lambda, \lambda', \lambda'')|^2 \times [2(n_{\vec{\lambda}} - n_{\vec{\lambda}''})\delta(\omega(\lambda) + \omega(\lambda') - \omega(\lambda'')) + (1 + n_{\vec{\lambda}} + n_{\vec{\lambda}''})\delta(\omega(\lambda) - \omega(\lambda') - \omega(\lambda''))]$$
(2)

where $V_3(-\lambda,\lambda',\lambda'')$ are the three-phonon coupling matrix elements. The first delta function in the above equation represents the absorption scattering process and the second delta function represents the decay process.

DFT calculations were carried out using QUANTUM-ESPRESSO.²⁵ Norm-conserving pseudopotentials in the localdensity approximation (LDA) were used with a plane-wave cut-off of 100 Ry. A Monkhorst²⁶ k-point mesh of $12 \times 12 \times 12$ was used to describe the electronic properties. The 8 \times 8 \times 8 q-grid was used to compute the dynamical matrices and the 2nd order IFCs. The 3rd order IFCs were computed using D3Q18,19,27 package, on a $4 \times 4 \times 4$ supercell. Acoustic sum rules were imposed on both 2nd and 3rd order force constants. Phonon linewidth and k calculations were carried out on a 30 \times 30 \times 30 g-mesh. For the exact solution of PBTE, typically 10 iterations were found to be sufficient to achieve convergence.¹⁸

The lattice parameter of unstrained BP was determined through energy minimization to be $a_0 = 4.468$ Å. Computed phonon dispersion (in good agreement with the experimental measurements²⁸) for unstrained cases is shown in Fig. 2c. For the strained cases, the lattice was compressed by 2% and 4% in the x-y plane (along both x and y directions) and relaxed in the z-direction (Fig. 2b). The lattice dimensions obtained after relaxing the structure correspond to a Poisson ratio of 0.19, in good agreement with the reported values.29

As the lattice is biaxially compressed, the phonon band gap between acoustic and optical phonons increases from 148 cm⁻¹ for the unstrained case to 157 cm⁻¹ and 168.0 cm⁻¹ for 2% and 4% compressive strains, respectively (Fig. 2c). This increase in band gap increases k (Fig. 3a). At 300 K, while in-plane (defined as the plane in which compressive biaxial strain is applied) k of unstrained BP is computed to be 591 W m⁻¹ K⁻¹, for 2% and 4% strained BP, in-plane k is found to be enhanced to values of 699 W m⁻¹ K⁻¹ and 802.5 W m⁻¹ K⁻¹ (Fig. 3a), representing an increase of 18.3% and 35.8%, respectively, over unstrained BP (anisotropy in bulk k is found to be small). The value of 802.5 W m^{-1} K $^{-1}$ obtained for 4% strained BP is almost 5-times the k of silicon²⁰ ($k = 155 \text{ W m}^{-1} \text{ K}^{-1}$ at 300 K), providing avenues to significantly enhance the heat dissipation in nanoelectronic applications. Fig. 3b shows that k is significantly enhanced at a nanoscale. At L = 200 nm, an increase in out-of-plane k of 25% is observed at 300 K (Fig. 3b), from 120.6 W m⁻¹ K⁻¹, for strain, ε = 0%, to 150.4 W m⁻¹ K⁻¹, for ε = 4%. This enhanced value at

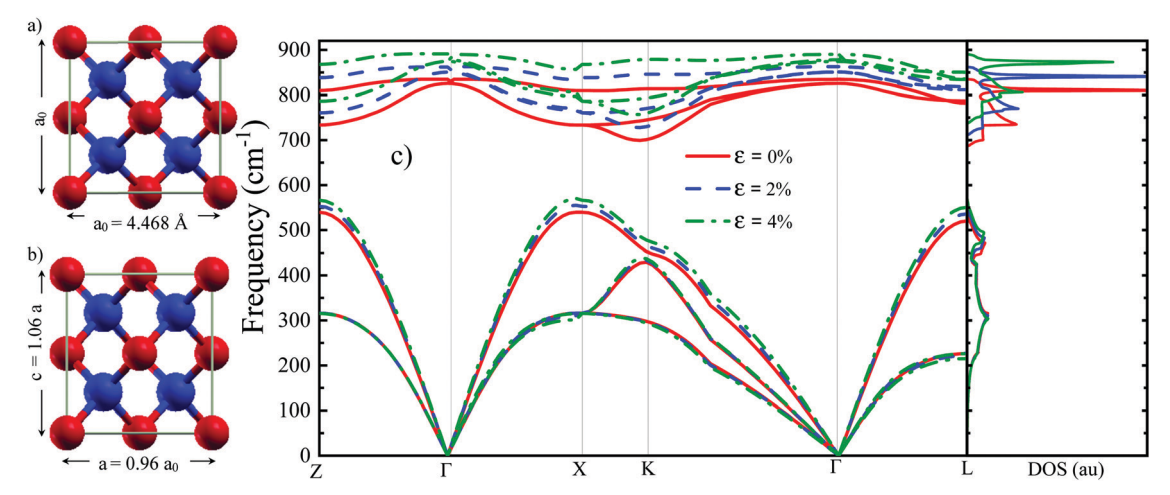


Fig. 2 Cubic boron-phosphide with (a) zero strain and (b) biaxial strain of 4%, (c) phonon dispersion and density of states for the 0%, 2% and 4% biaxially strained BP

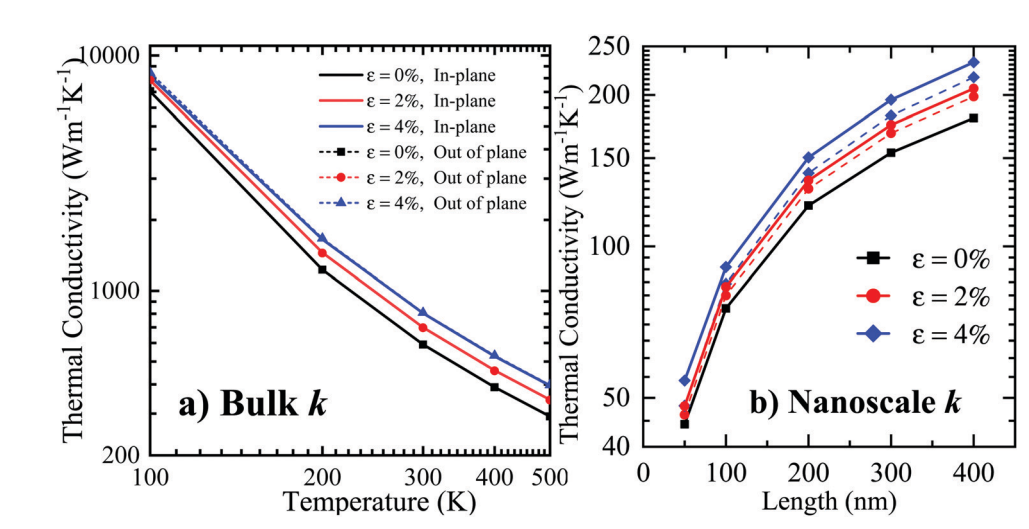


Fig. 3 (a) Computed thermal conductivity of 0%, 2% and 4% biaxially strained BP obtained by exactly solving PBTE, (b) enhancement in k at nanometer length scales in strained BP at 300 K. Dashed lines represent the in-plane (plane in which biaxial compression is applied) k, while solid lines represent the out-of-plane k.

 $\varepsilon = 4\%$ is almost equal to the bulk k value of silicon. ²⁰ At 400 nm, the increase in k is even higher, by almost 30%, from 180 W m⁻¹ K⁻¹ to 232.5 W m⁻¹ K⁻¹, for the same increase in strain (Fig. 3b). These large increases in nanoscale k point to the potential of applying biaxial strain for enhancement of nanoscale heat dissipation in electronic applications (k values at nanometer length scales were achieved by introducing additional Casimir scattering,³⁰ $1/\tau_{\text{boundary}} = |\mathbf{v}|/L$, where ν is the phonon velocity and L is the system size, in the solution of PBTE).

We first describe an increase in the bulk k (seen in Fig. 3a) by comparing the phonon scattering rates and group velocities of longitudinal acoustic (LA) and transverse acoustic (TA) phonons for unstrained and strained BP in Fig. 4 (ignoring optical phonons which are found to contribute less than 0.5% to overall k). Strain significantly decreases the scattering rates (Fig. 4a) and increases the group velocities (Fig. 4b) of acoustic

phonons. At a frequency of ~ 250 cm⁻¹, the mean phonon linewidth of TA and LA modes in 4% strained BP is lower by 42% and 60%, relative to 0% strain case at 300 K (Fig. 4c and d). A significant increase in group velocities in strained BP is also visible in Fig. 4b, particularly for the LA phonons. These effects, a decrease in scattering and an increase in group velocities, together enhance bulk k. To approximately separate the effect of two on k enhancement, we recomputed k for hypothetical 4% strain case by imposing the linewidths to be the same as 0% case (but using the real velocities of 4% case). This resulted in a k, higher by only 12.8%, relative to 0% case, suggesting that the decrease in phonon scattering rates (seen in Fig. 4a, c and d) is the dominant effect contributing to the observed 36% k enhancement in 4% strained BP.

The strain enhanced phonon band gap (Fig. 2c) leads to the above decrease in phonon scattering rates in biaxially compressed

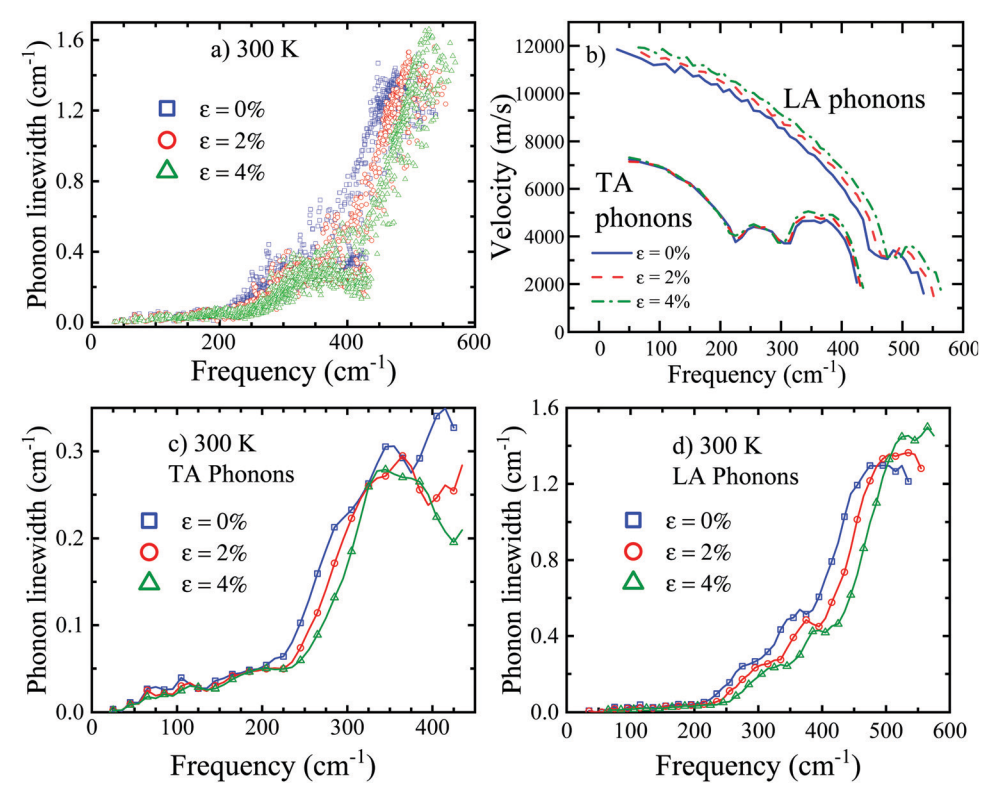


Fig. 4 (a) Comparison of phonon linewidths in unstrained and strained BP at 300 K, (b) mean phonon velocities at different frequencies for LA and TA phonons at different strains. Comparison of mean linewidths of (c) TA phonons and (d) LA phonons in unstrained and strained BP at 300 K.

BP, as described next. Fig. 5a and b show that the linewidths of both LA and TA modes decrease with the increasing strain along Γ -X. In Fig. 5c and d, we investigate the following four scattering channels in scattering of LA and TA phonons – (a) $a + a \rightarrow o$, (b) $a + o \rightarrow o$, (c) $a + a \rightarrow a$, and (d) $a \rightarrow a + a$ (a channel such as $a + a \rightarrow o$ represents the scattering of an acoustic phonon by absorbing another acoustic phonon yielding an optical phonon, whereas a channel such as $a \rightarrow a + a$ represents the decay of an acoustic phonon into two lower frequency acoustic phonons). For large part of Γ -X, the most significant contribution to scattering of LA and TA phonons in BP is from the $a + a \rightarrow o$ scattering channel (Fig. 5c and d). At zone edge (point X), the $a + a \rightarrow o$ channel contributes 97.5% and 85.2% to the total scattering rate of TA (Fig. 5d) and LA (Fig. 5c) modes, respectively.

Strain leads to a large decrease in magnitude of this dominant $a + a \rightarrow o$ channel for TA mode along the Γ -X direction (Fig. 5f). The role of the strain mediated larger phonon band gap in decreasing the $a + a \rightarrow o$ scattering in strained BP (Fig. 5f) can be seen through an example, by considering that in the unstrained case, a TA phonon of frequency $\omega = 148 \text{ cm}^{-1}$ can scatter by absorbing an LA phonon of frequency $\omega' = 540 \text{ cm}^{-1}$, yielding the lowest energy optical phonon of frequency $\omega'' = 688 \text{ cm}^{-1}$, thus satisfying energy conservation, $\omega + \omega' = \omega''$ (provided the momentum conservation is satisfied) (Fig. 2c). In the 2% strained case, however, due to the increase in the phonon band gap, this scattering channel becomes forbidden, since the optical phonon frequencies are higher than 688 cm⁻¹ (Fig. 2c), thus violating energy conservation. This dramatically

suppresses the phonon scattering through the $a + a \rightarrow o$ channel in strained BP. At Brillouin zone edge (X-point), for example, strain leads to a decrease in the strength of this channel for TA modes by 16.1% and 28% for 2% and 4% strain, respectively, relative to 0% strain (Fig. 5f). For LA phonon mode (Fig. 5e), the $a + a \rightarrow o$ scattering again decreases for most part of Γ -X, except close to the Brillouin zone edge (near X) (the cause of increase in $a + a \rightarrow o$ scattering for LA modes in a small region near zone edge, as well as comparison of scattering channels for the entire Brillouin zone, is presented in the ESI†). This decrease in scattering increases the heat conduction by LA and TA phonons in strained BP. Overall, while LA and TA phonons contribute 137.0 W m⁻¹ K⁻¹ and 399.3 W m⁻¹ K⁻¹ to total k in unstrained BP at 300 K, their heat conduction increases by 20.3% and 17.6%, respectively, in 2% strained BP and by 41.8% and 33.8%, respectively, in 4% strained BP, relative to the 0% strain case.

Nanoscale k enhancement (Fig. 3b) can now be understood by observing that a strain mediated decrease in the $a + a \rightarrow o$ scattering is particularly dominant at higher frequencies exceeding 200 cm⁻¹ (Fig. 4a, c and d) and higher wavevectors (Fig. 5e and f), as described next. At small wavevectors, the frequencies of acoustic phonons are too small to allow scattering into higher frequency optical phonons through the $a + a \rightarrow o$ channel, causing the contribution of the $a + a \rightarrow o$ channel to overall scattering to be weak. Note that the $a + a \rightarrow o$ scattering is completely forbidden in unstrained BP below frequencies of 148 cm⁻¹, equal to the phonon band gap, since a minimum of

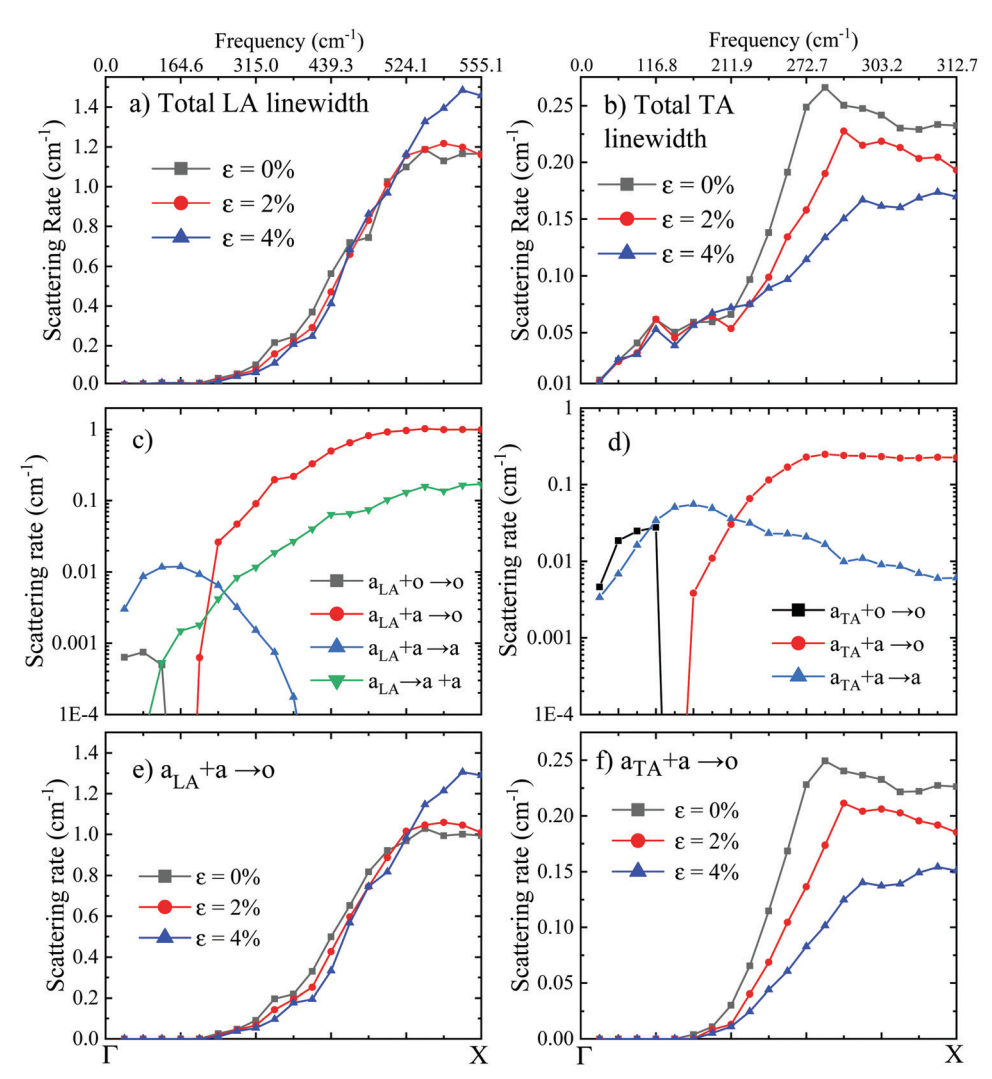


Fig. 5 (a) Comparison of total phonon linewidth of phonons along $\Gamma - X$ in unstrained and strained BP at 300 K for (a) LA (longitudinal acoustic) and (b) TA (transverse acoustic) modes. Contribution of dominant scattering channels at 300 K to total scattering rate in unstrained BP for (c) LA and (d) TA modes. Comparison of scattering at 300 K due to (e and f) $a + a \rightarrow o$ channel. The top scale represents the average of the frequencies of LA and TA phonons in 0%, 2% and 4% strained BP along Γ -X.

 $148~{
m cm}^{-1}$ is needed to absorb another acoustic phonon to reach the lowest frequency optical phonon, $\omega_{\min}^{\text{acoustic}}$ (148 cm⁻¹) + $\omega_{\rm max}^{\rm acoustic}$ (540 cm⁻¹) = $\omega_{\rm min}^{\rm optical}$ (688 cm⁻¹). An increase in frequency makes the energy conservation for the $a + a \rightarrow o$ channel progressively more feasible, causing the contribution of this channel to increase at higher frequencies. The increase in the phononic band gap in strained BP, now by suppressing this large $a + a \rightarrow o$ channel contribution to scattering at higher frequencies (Fig. 5e and f), thus also facilitates a large decrease in overall scattering rates at higher frequencies $> 200 \text{ cm}^{-1}$ (Fig. 4a). This effect is also seen to manifest as an increase in spectral contribution to k from higher frequency phonons in strained BP (Fig. 6c). In 4% strained BP, for example, phonon of frequencies >200 cm⁻¹ contribute 445.1 W m⁻¹ K⁻¹ (55.5%) to overall k, significantly higher relative to unstrained BP, where the corresponding phonons only contribute 278.9 W m⁻¹ K⁻¹ (47.2%).

The enhancement in nanoscale k is directly related to the above-mentioned increase in thermal transport at higher frequencies. Phonon meanfreepaths $(\Lambda_{\lambda} = \tau_{\lambda} \nu_{\lambda})$ generally decrease with an increase in frequency due to the increase in scattering, being in the micron range at lower frequencies <100 cm⁻¹ in BP (see Fig. 6a and b). At higher frequencies >200 cm⁻¹ (where $a + a \rightarrow o$ channel is active), Fig. 6a and b show that Λ in unstrained BP is mostly in the nanometer range (Λ for TA phonons is seen to be below 600 nm) and contributes strongly to k at nanoscale lengths. A decrease in the $a + a \rightarrow o$ scattering at these higher frequencies then enhances both TA and LA phonon meanfreepaths in the nanometer regime (Fig. 6a and b).

k at any length scale L is primarily an aggregate of heat conduction by phonon modes λ with meanfreepaths (Λ_{λ}) lower than $L(k_L \propto \sum_{i}^{\Lambda_{\lambda} < L} C_{\lambda} \nu_{\lambda} \Lambda_{\lambda}, C_{\lambda})$ is the specific heat of mode λ

(since higher meanfreepath phonons get scattered at the boundaries). The above-mentioned increase in meanfreepaths in the nanometer regime (through a decrease in scattering which enhances phonon lifetimes τ_{λ}) seen in Fig. 6a and b

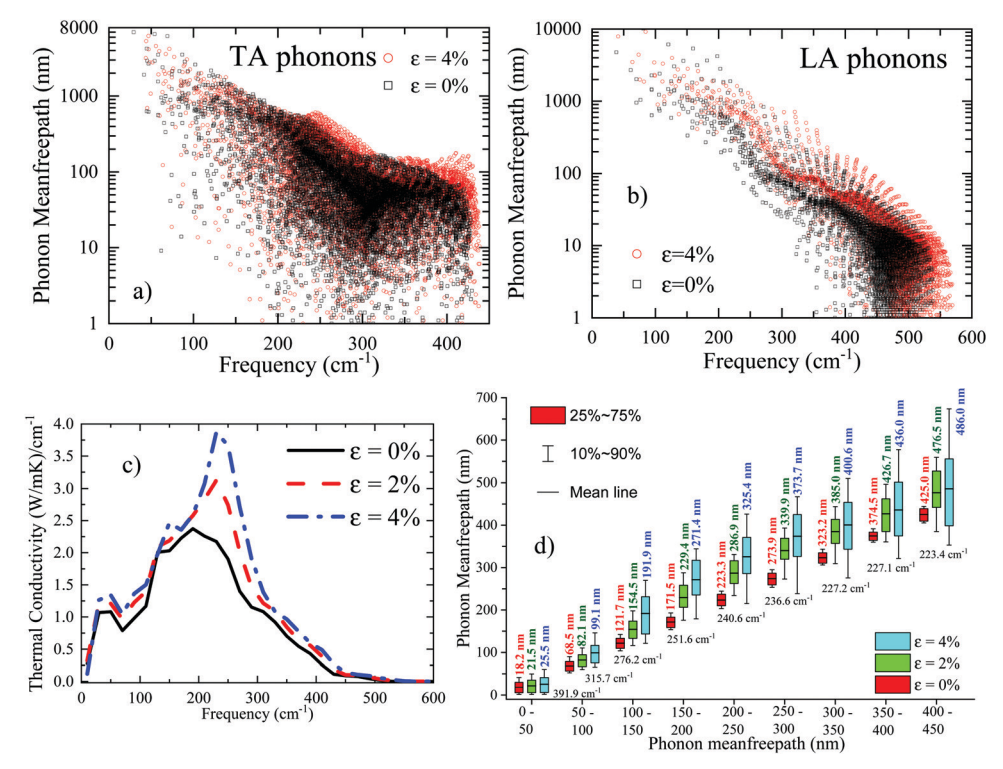


Fig. 6 Phonon meanfreepaths as a function of frequency in unstrained and strained BP of (a) TA phonons and (b) LA phonons. (c) Spectral dependence of thermal conductivity in unstrained and strained BP and (d) change in meanfreepaths of phonons in strained BP; values above boxes represent the average mean-freepath, while values below are the mean frequencies for the particular group of phonons.

enhances their *k* contribution at nanoscale lengths (since $k_{\lambda} \propto \Lambda_{\lambda}$), thus leading to enhancement in k in the nanometer regime (seen in Fig. 3b). The increase in Λ is seen more clearly in Fig. 6d, where we select phonons in different meanfreepath ranges in unstrained BP, such as 0-50 nm, 50-100 nm and up to 400-450 nm, and study changes in Λ of the same group of phonons in strained BP. Fig. 6d shows an increase in Λ in each group, leading to the enhancement in k at all nanometer length scales presented in Fig. 3b. Above analysis clearly demonstrates that a decrease in the $a + a \rightarrow o$ scattering at higher frequencies, where phonon meanfreepaths are in nanometers, leads to an enhancement in k at nanometer length scales in strained BP. The presented effect of strain mediated increase in Λ at nanometer lengths through suppression of anharmonic scattering at higher frequencies can be applied to enhance nanoscale k in a wide range of compound semiconductors with a phononic band gap in their vibrational spectra. Such high ksemiconductors can function as efficient heat spreaders, thus improving the thermal management.

Note that the effect is related to the magnitude of the phonon band gap, which determines the frequencies and therefore Λ at which the $a + a \rightarrow o$ scattering is dominant, thus determining the length scales at which Λ and k can be enhanced. This can be employed to tune k enhancement at particular nanometer length scales in different compound semiconductors through differences in their phonon band gaps. Biaxial strain investigated in this work can be achieved by growth of a material on a lattice mismatched substrate,³¹

further providing avenues for applications of the outlined effect in nanoelectronics. Finally, it is noted that thermal conductivities reported in this work are computed based on the lowest order three-phonon scattering, ignoring the role of fourphonon processes, which have been shown to have a minimal impact on k of BP in a recent work.³²

In summary, by deriving harmonic and anharmonic interatomic force interactions, from density functional theory and using them along with an exact solution of the Boltzmann transport equation, we have provided a microscopic description of enhancement in nanoscale thermal conductivity in biaxially strained boron phosphide. At 200 nm, an increase in out-ofplane k of 25% is observed at 300 K, from 120.6 W m⁻¹ K⁻¹, for strain $\varepsilon = 0\%$, to 150.4 W m⁻¹ K⁻¹, for $\varepsilon = 4\%$. Bulk k of 4% biaxially compressed boron-phosphide (BP) is also found to be enhanced to 802.5 W m⁻¹ K⁻¹ at 300 K, almost 35.8% higher than 591 W m⁻¹ K⁻¹, computed for unstrained BP, and almost 5-fold the k of silicon Si. The increase in the phonon band gap in strained BP suppresses the dominant scattering channel involving scattering of acoustic phonons through absorption of other acoustic phonons into optical phonons $(a + a \rightarrow o$ channel), enhancing phonon lifetimes and thus k of the material. Furthermore, the $a + a \rightarrow o$ channel is dominant at higher frequencies; suppression of scattering at these higher frequencies enhances the phonon meanfreepaths in the nanometer range, thus enhancing nanoscale k. These results have important implications for achieving efficient thermal management in nanoelectronic applications.

Conflicts of interest

PCCP

There are no conflicts of interest to declare.

Acknowledgements

RM and JG acknowledge support from the National Science Foundation CAREER award under Award No. #1847129. We also acknowledge OU Supercomputing Center for Education and Research (OSCER) for providing computing resources for this work.

References

- D. G. Cahill, P. V. Braun, G. Chen, D. R. Clarke, S. Fan, K. E. Goodson, P. Keblinski, W. P. King, G. D. Mahan, A. Majumdar, H. J. Maris, S. R. Phillpot, E. Pop and L. Shi, Nanoscale thermal transport. II. 2003–2012, *Appl. Phys. Rev.*, 2014, 1(1), 011305.
- 2 G. Chen, Nonlocal and Nonequilibrium Heat Conduction in the Vicinity of Nanoparticles, *J. Heat Transfer*, 1996, 118(3), 539–545.
- 3 B. Poudel, Q. Hao, Y. Ma, Y. Lan, A. Minnich, B. Yu, X. Yan, D. Wang, A. Muto, D. Vashaee, X. Chen, J. Liu, M. S. Dresselhaus, G. Chen and Z. Ren, High-Thermoelectric Performance of Nanostructured Bismuth Antimony Telluride Bulk Alloys, *Science*, 2008, 320(5876), 634.
- 4 H. Zhang, C. Hua, D. Ding and A. J. Minnich, Length Dependent Thermal Conductivity Measurements Yield Phonon Mean Free Path Spectra in Nanostructures, *Sci. Rep.*, 2015, 5(1), 9121.
- 5 Y. Liu, S. Zhang, Z. Han and Y. Zhao, Grain-size-dependent thermal conductivity of nanocrystalline materials, *J. Nanopart. Res.*, 2016, **18**(10), 296.
- 6 J. de Boor, D. S. Kim, X. Ao, D. Hagen, A. Cojocaru, H. Föll and V. Schmidt, Temperature and structure size dependence of the thermal conductivity of porous silicon, *Europhys. Lett.*, 2011, 96(1), 16001.
- 7 L. Lindsay, D. A. Broido and T. L. Reinecke, First-Principles Determination of Ultrahigh Thermal Conductivity of Boron Arsenide: A Competitor for Diamond?, *Phys. Rev. Lett.*, 2013, 111(2), 025901.
- 8 L. Lindsay, D. A. Broido and T. L. Reinecke, Phonon-isotope scattering and thermal conductivity in materials with a large isotope effect: a first-principles study, *Phys. Rev. B: Condens. Matter Mater. Phys.*, 2013, **88**(14), 144306.
- 9 L. Lindsay, D. A. Broido and T. L. Reinecke, Thermal Conductivity and Large Isotope Effect in GaN from First Principles, *Phys. Rev. Lett.*, 2012, **109**(9), 095901.
- 10 F. Tian, B. Song, X. Chen, N. K. Ravichandran, Y. Lv, K. Chen, S. Sullivan, J. Kim, Y. Zhou, T.-H. Liu, M. Goni, Z. Ding, J. Sun, G. A. G. Udalamatta Gamage, H. Sun, H. Ziyaee, S. Huyan, L. Deng, J. Zhou, A. J. Schmidt, S. Chen, C.-W. Chu, P. Y. Huang, D. Broido, L. Shi, G. Chen and Z. Ren, Unusual high thermal conductivity in boron arsenide bulk crystals, *Science*, 2018, 361(6402), 582.

- 11 K. Chen, B. Song, N. K. Ravichandran, Q. Zheng, X. Chen, H. Lee, H. Sun, S. Li, G. A. Gamage, F. Tian, Z. Ding, Q. Song, A. Rai, H. Wu, P. Koirala, A. J. Schmidt, K. Watanabe, B. Lv, Z. Ren, L. Shi, D. G. Cahill, T. Taniguchi, D. Broido and G. Chen, Ultrahigh thermal conductivity in isotope-enriched cubic boron nitride, *Science*, 2020, eaaz6149.
- 12 D. A. Broido, L. Lindsay and T. L. Reinecke, Ab initio study of the unusual thermal transport properties of boron arsenide and related materials, *Phys. Rev. B: Condens. Matter Mater. Phys.*, 2013, **88**(21), 214303.
- 13 J. Garg, N. Bonini and N. Marzari, High Thermal Conductivity in Short-Period Superlattices, *Nano Lett.*, 2011, **11**(12), 5135–5141.
- 14 N. K. Ravichandran and D. Broido, Non-monotonic pressure dependence of the thermal conductivity of boron arsenide, *Nat. Commun.*, 2019, **10**(1), 827.
- 15 Q. Zheng, S. Li, C. Li, Y. Lv, X. Liu, P. Y. Huang, D. A. Broido, B. Lv and D. G. Cahill, High Thermal Conductivity in Isotopically Enriched Cubic Boron Phosphide, *Adv. Funct. Mater.*, 2018, 28(43), 1805116.
- 16 J. S. Kang, H. Wu and Y. Hu, Thermal Properties and Phonon Spectral Characterization of Synthetic Boron Phosphide for High Thermal Conductivity Applications, *Nano Lett.*, 2017, 17(12), 7507–7514.
- 17 L. Lindsay, D. A. Broido, J. Carrete, N. Mingo and T. L. Reinecke, Anomalous pressure dependence of thermal conductivities of large mass ratio compounds, *Phys. Rev. B: Condens. Matter Mater. Phys.*, 2015, **91**(12), 121202.
- 18 G. Fugallo, M. Lazzeri, L. Paulatto and F. Mauri, Ab initio variational approach for evaluating lattice thermal conductivity, *Phys. Rev. B: Condens. Matter Mater. Phys.*, 2013, 88(4), 045430.
- 19 L. Paulatto, F. Mauri and M. Lazzeri, Anharmonic properties from a generalized third-order ab initio approach: theory and applications to graphite and graphene, *Phys. Rev. B: Condens. Matter Mater. Phys.*, 2013, **87**(21), 214303.
- 20 D. A. Broido, M. Malorny, G. Birner, N. Mingo and D. A. Stewart, Intrinsic lattice thermal conductivity of semiconductors from first principles, *Appl. Phys. Lett.*, 2007, 91(23), 231922.
- 21 J. Garg, N. Bonini, B. Kozinsky and N. Marzari, Role of Disorder and Anharmonicity in the Thermal Conductivity of Silicon-Germanium Alloys: A First-Principles Study, *Phys. Rev. Lett.*, 2011, **106**(4), 045901.
- 22 A. Debernardi, S. Baroni and E. Molinari, Anharmonic Phonon Lifetimes in Semiconductors from Density-Functional Perturbation Theory, *Phys. Rev. Lett.*, 1995, 75(9), 1819–1822.
- 23 G. Deinzer, G. Birner and D. Strauch, *Ab initio* calculation of the linewidth of various phonon modes in germanium and silicon, *Phys. Rev. B: Condens. Matter Mater. Phys.*, 2003, **67**(14), 144304.
- 24 G. P. Srivastava, *Physics of Phonons*, Taylor and Francis Group, New York, 1990.
- 25 P. Giannozzi, S. Baroni, N. Bonini, M. Calandra, R. Car, C. Cavazzoni, D. Ceresoli, G. L. Chiarotti, M. Cococcioni, I. Dabo, A. Dal Corso, S. de Gironcoli, S. Fabris, G. Fratesi, R. Gebauer, U. Gerstmann, C. Gougoussis, A. Kokalj, M. Lazzeri, L. Martin-Samos, N. Marzari, F. Mauri,

- R. Mazzarello, S. Paolini, A. Pasquarello, L. Paulatto, C. Sbraccia, S. Scandolo, G. Sclauzero, A. P. Seitsonen, A. Smogunov, P. Umari and R. M. Wentzcovitch, QUANTUM ESPRESSO: a modular and open-source software project for quantum simulations of materials, J. Phys.: Condens. Matter, 2009, 21(39), 395502.
- 26 H. J. Monkhorst and J. D. Pack, Special points for Brillouinzone integrations, Phys. Rev. B: Solid State, 1976, 13(12), 5188-5192.
- 27 L. Paulatto, I. Errea, M. Calandra and F. Mauri, Firstprinciples calculations of phonon frequencies, lifetimes, and spectral functions from weak to strong anharmonicity: the example of palladium hydrides, Phys. Rev. B: Condens. Matter Mater. Phys., 2015, 91(5), 054304.

- 28 H. W. L. Alves and K. Kunc, Lattice dynamics of boron phosphide, J. Phys.: Condens. Matter, 1992, 4(31), 6603-6612.
- 29 S. Daoud, N. Bioud, L. Belagraa and N. Lebgaa, Elastic, Optoelectronic, and Thermal Properties of Boron Phosphide, J. Nano Electron. Phys., 2013, 5, 04061.
- 30 H. B. G. Casimir, Note on the conduction of heat in crystals, Physica, 1938, 5(6), 495-500.
- 31 M. Clavel, P. Goley, N. Jain, Y. Zhu and M. K. Hudait, Strain-Engineered Biaxial Tensile Epitaxial Germanium for High-Performance Ge/InGaAs Tunnel Field-Effect Transistors, IEEE J. Electron Devices Soc., 2015, 3(3), 184-193.
- 32 N. K. Ravichandran and D. Broido, Phonon-Phonon Interactions in Strongly Bonded Solids: Selection Rules and Higher Order Processes, Phys. Rev. X, 2020, 10, 021063.